Version of Record: https://www.sciencedirect.com/science/article/pii/S0034425716300074
Manuscript_5e6e809d513c3205285f328aea3d3f27

Comparison of Landsat 8 and Landsat 7 for Regional Measurements of CDOM and Water Clarity in Lakes

Leif G. Olmanson[a,*], Patrick L. Brezonik[b], Jacques C. Finlay[c] and Marvin E. Bauer[a]

[a] *Department of Forest Resources, University of Minnesota, St. Paul, MN 55108*
[b] *Department of Civil, Environmental and Geo-Engineering, University of Minnesota, Minneapolis, MN 55445*
[c] *Department of Ecology, Evolution, and Behavior, University of Minnesota, St. Paul, MN 55108*

Corresponding Author: Department of Forest Resources, University of Minnesota, St. Paul, MN 55108.

Tel. +1 651-206-9102

Email address: olman002@umn.edu (L. G. Olmanson)

Abstract

The potential strengths and limitations of the Landsat systems for water clarity and colored dissolved organic matter (CDOM) measurement were evaluated in Minnesota in the summers of 2013 and 2014. Optical water quality characteristics, including chlorophyll *a*, total suspended solids (TSS), dissolved organic carbon (DOC), and CDOM were collected along with imagery from Landsats 7 and 8. Sites represented a wide range of concentrations of CDOM, chlorophyll, and mineral suspended solids (MSS), the primary factors that affect reflectance. Clear images from September 24, 2013 (Landsat 7) and September 16, 2013 (Landsat 8) acquired for northern Minnesota eight days apart allowed comparison of the respective ETM+ and OLI sensors for CDOM measurements. We examined a wide variety of potential band and band ratio models and found some two-variable models that included the NIR band worked well for Landsat 8 (R^2 = 0.82) and reasonably well for Landsat 7 (R^2 = 0.74). The commonly used green/red model had a poor fit for both sensors (R^2 = 0.24, 0.25), and five sites with high MSS were clear outliers. Exclusion of these sites and other sites not included with the Landsat 7 dataset yielded a less optically complex subset of 20 coincident lakes. For this subset strong models were found for many band and band ratio models, including the commonly used green/red model with R^2 = 0.79 for Landsat 7 and R^2 = 0.81 for Landsat 8. The less optically complex subset may explain why the green/red model has worked well in other areas. For optically complex waters CDOM models that used the new Landsat 8 ultra-blue and narrower NIR band worked best for the full dataset indicating that the new bands and other Landsat 8 characteristics, such as higher radiometric sensitivity and improved signal-to-noise ratios, improve CDOM measurements.

For water clarity measured as Secchi depth (SD), we compared September 1, 2008 Landsat 7 and August 22, 2013 Landsat 8 images from path 28 using stepwise regression to identify the

best model using all bands and band ratios including the new blue and narrower NIR band. The best water clarity model for Landsat 8 used the OLI 2/4 band ratio plus OLI band 1 and was nearly identical with a model using the OLI 2/4 band ratio plus OLI band 2. The latter model is similar to the model used for previous Landsat water clarity assessments, which used the ETM+ 1/3 band ratio plus ETM+ band 1. For SD measurements we found strong relationships with both sensors, with only slight improvements for the OLI sensor for the lakes in our datasets. In contrast to some previous reports that indicated Landsat 7's ETM+ lacked sufficient sensitivity for reliable retrieval of CDOM, we found that overall both sensors worked well for water clarity and CDOM measurements. This will allow their continued use for current and historical measurements of important water characteristics on a regional scale.

1. Introduction

Historic and recent water clarity assessments in the Midwest USA based on Landsat 4, 5, and 7 imagery (Olmanson et al., 2008; Chipman et al., 2004; Greb et al., 2009; Fuller et al., 2004 & 2011) have been used to determine spatial and temporal patterns on > 25,000 lakes and evaluate factors that affect water clarity (Olmanson et al., 2013). Landsat 8 will allow continuation of these assessments and potentially may enhance them. Improved capabilities of Landsat 8 data, including an additional shorter wavelength blue band (ultra-blue), narrower near-infrared (NIR) band, 12-bit radiometric resolution, and greater signal to noise ratios, could increase abilities to monitor high clarity lakes, which have inherently low reflectance in the blue and red bands typically used for retrieval of Secchi depth, a common measurement of water clarity. The same improvements in the OLI sensor also suggest Landsat 8 data has the potential to improve measurement of other water quality parameters, such as CDOM (colored dissolved organic matter), which constitutes the major fraction of DOM in many natural waters.

The primary objective of this study was to compare the capabilities of Landsat 8 to that of Landsat 7 for retrieving two important optical water quality variables: Secchi depth (SD), a measure of water clarity, and CDOM, an optical proxy for dissolved organic carbon (DOC) concentration. To do this we conducted field campaigns on lakes and rivers in Minnesota during the summers of 2013 and 2014 and measured the following optical water quality characteristics: chlorophyll *a*, total suspended solids (TSS), dissolved organic carbon (DOC), and CDOM, as well as in situ reflectance spectra. Sites were selected to obtain a wide range of concentrations of CDOM, chlorophyll, and mineral suspended solids (MSS), the primary factors that affect light reflectance from water. Relatively clear images of path 27 for Landsat 7 (September 24, 2013) and 8 (September 16, 2013) in northern Minnesota that include many of the sampled lakes were

acquired eight days apart. A high likelihood of similar water quality conditions over this period facilitated a comparison of the two sensors (ETM+ on Landsat 7 and OLI on Landsat 8) for CDOM measurements. Because SD is measured throughout the state on a regular basis, we selected imagery that covered a larger area to increase the number and range of SD data for our analysis. We used a September 1, 2008 Landsat 7 image that we had previously used as part of a statewide assessment and an August 22, 2013 Landsat 8 image from path 28 for comparison.

2. Background

2.1 Water clarity

Water clarity as measured by Secchi disk transparency (commonly referred to as Secchi depth, SD) is the most widely measured lake water quality parameter. Its simplicity and low cost facilitates its use by many citizen monitoring programs. SD is important because it relates directly to water quality as perceived by lake users and to chlorophyll levels and trophic condition. An important optical property of natural waters, SD,is affected by both light absorption and scattering. In most inland lakes of the Midwestern USA, phytoplankton and plankton-derived particles control SD, and it is commonly used as a simple measure of lake trophic status. Many studies have shown strong inverse correlations between SD and chlorophyll levels in lakes (Carlson, 1977; Olmanson et al., 2011).

For inland lakes SD is also the water quality characteristic most widely measured by remote sensing (e.g., Olmanson et al., 2008; Greb et al., 2009). This situation is based largely on three factors: (i) Landsat has been the only inexpensive, regularly collected imagery with adequate spatial resolution for all lakes > 4 ha, (ii) Landsat sensors are able to retrieve accurate SD data using Landsat's spectral bands, and (iii) Landsat's sensors do not have adequate spectral characteristics for chlorophyll measurements in optically complex inland waters because

suspended solids cannot be distinguished from chlorophyll in the Landsat sensors (Olmanson et al. 2015).

2.2 CDOM

Colored dissolved organic matter (CDOM) is the most abundant DOM fraction in many natural waters (e.g., Thurman, 1983; Davies-Colley and Vant, 1987), especially in forested watersheds with wetlands. It affects water quality through mobilization of metals and hydrophobic chemicals, and it serves as a major source of reactive photochemical intermediates that control the photolysis of both natural DOM and trace organic contaminants, such as pharmaceuticals and personal care products. CDOM controls many aquatic ecosystem processes; for example, it affects light penetration and thus limits primary production, and it affects the thermal properties of water bodies (Houser, 2006). CDOM also has negative effects on production of safe drinking water and is a major precursor for trihalomethanes and other disinfection by-products. CDOM levels are needed for regional and global-scale models of carbon cycling because freshwater lakes play a much more important role in carbon cycling than might be anticipated from the small fraction of land area they occupy (Wilkinson et al., 2013).

Although CDOM is a critically important water quality characteristic, few water management agencies include CDOM in their routine water quality monitoring programs. The paucity of CDOM data limits our understanding of carbon cycling in surface waters in many regions. Optical remote sensing via satellite imagery has the potential to fill this void and improve our understanding of CDOM distribution and the environmental factors that affect CDOM and DOM levels in surface waters.

CDOM is usually reported as the absorptivity, a_λ, of filtered water (0.2-0.7 μm pore size filter) at a specified wavelength; i.e., a_λ (units of m^{-1}) = $2.303A_\lambda/\ell$, where A_λ = absorbance of

filtered water measured spectrophotometrically at wavelength λ and ℓ = light path length (m). Unfortunately, no standard wavelength is in use; marine scientists use 412 nm, and freshwater scientists usually use 420 or 440 nm, but other wavelengths also are used.

The Landsat series of satellites (1-8) has collected imagery since the 1970s, and most of it has been archived, potentially enabling assessment of historical trends in CDOM levels on water bodies lacking field monitoring data. Several studies over the past decade have described empirical band-ratio algorithms to retrieve CDOM data from satellite imagery, e.g., Kutser et al. (2005a,b):

$$a_{420} = 5.13(\text{ALI2}/\text{ALI3})^{-2.67} \quad (R^2 = 0.73;\ n = 26) \qquad [1]$$

ALI2 and ALI3 in eq. 1 represent reflectance (R) in Advanced Land Imager bands 2 (525-605 nm) and 3 (630-690 nm). Menken et al. (2006) found a similar retrieval equation using ground-based hyperspectral reflectance data:

$$a_{440} = 166(R_{670}/R_{571})^{2.29} \quad (R^2 = 0.74\text{-}0.88;\ n = 13\text{-}15) \qquad [2]$$

The higher R^2 was obtained when two lakes with very high chlorophyll (> 200 μg/L) and suspended solids concentrations (> 80 mg/L) were excluded from the regression. Ficek et al. (2011) also reported an equation of similar form to eq. (1) with $R^2 = 0.85$ (n = 235) using a ground-based spectroradiometer and the ratio of reflectance values at 570 and 655 nm to retrieve CDOM data on Pomeranian lakes in eastern Poland.

Brezonik et al. (2005) found that Landsat 5 TM yielded a poor fit (low R^2) to CDOM data when the regression equations were based solely on reflectance ratios, but they found an R^2 of 0.77 (n = 15) using a two-term equation: $\ln(a_{440}) = b_0 + b_1\text{TM1} + b_2(\text{TM1}/\text{TM4})$. Similarly, Kutser (2012) found a weak relationship with a high amount of scatter between the ratio of Landsat bands 2 and 3 and CDOM in 14 Swedish lakes with a_{420} ranging from < 1 to ~18 m^{-1};

the scatter was especially evident at higher levels. Kutser found a better fit (R^2 = 0.62) for data from Lake Mälaren, a large, multi-basin water body with low to moderate CDOM (a_{420} = ~1.0-3.5 m^{-1}) near Stockholm. He attributed the poor fit for the 14 lakes to the low radiometric sensitivity of the Landsat 4, 5, and 7 sensors and the fact that the water-leaving signal inherently is low in lakes with high CDOM levels. This suggests that historical Landsat sensors may be poorly suited to waters having high CDOM levels. Landsat 8, launched in 2013, along with the European Sentinel-2 launched in 2015 with a second planned for launch in 2016 and Sentinel-3 satellites planned for launch in late 2015 and 2017, have sensors with improved radiometric sensitivity, greater signal to noise ratios and better spectral resolution, thus potentially improving the capabilities to use optical remote sensing to map CDOM levels in inland waters.

Based on data from 30 Upper Midwest lakes with wide ranges of CDOM, chlorophyll and TSS and simulated Landsat 8 OLI bands from in situ reflectance hyperspectra, Brezonik et al. (2015) recently found that the best CDOM model for OLI bands was similar to eq. 1. With simulated bands of the Sentinel-2 and 3 satellite sensors, which have a larger selection of bands, ratios using bands near 500 and 750 nm worked the best. Simulated Landsat 8 OLI bands 3 and 4 calculated from the hyperspectra yielded a predictive equation for a_{440} with R^2 = 0.84. That the Landsat 8 bands worked nearly as well as the narrower Sentinel bands and hyperspectral bands probably reflects the fact that CDOM spectra are smooth and lack specific peaks or troughs in absorbance or reflectance.

3. Methods

3.1 Calibration data

Sampling sites. The only data available for CDOM comparisons were from our 2013 and 2014 field campaigns, which included 61 surface water sites (lakes and rivers) in Minnesota and northern Wisconsin. Sites were selected to obtain a wide range of CDOM in both CDOM-dominated systems and in optically complex waters where chlorophyll (algae) and mineral suspended solids also affect reflectance. The 2013 results were described previously by Brezonik et al. (2015). Because CDOM is more stable temporally than chlorophyll and water clarity (Brezonik et al., 2015) and our sample size was small, we used CDOM data collected in both 2013 and 2014 (if the site was not measured in 2013) for sites within the clear portions of the available Landsat imagery. This yielded a total of 30 sites in the area of the Landsat images with 28 usable data points for the September 16, 2013 Landsat 8 image, 25 usable data points for the September 24, 2013 Landsat 7 image, and 25 coincident data points between the images. One missing Landsat 7 data point was caused by the scan line corrector (SLC) data gap, and two sites had identifiable haze covering the sites in the Landsat 7 image. The other two missing sites for both images were river stations where the open water area was too narrow to provide pixels unaffected by terrestrial and bottom effects.

Sampling and field procedures. SD was measured with a standard 20-cm disk from the shady side of a boat using the average of the depths where the disk just disappears and re-appears when raised from below the depth of disappearance. Water samples for determination of DOC, CDOM, absorbance, and chlorophyll *a* were collected in glass bottles submerged ~20 cm below the water surface. Bottles used for water samples were cleaned by acid washing, rinsing three times with nanopure water, and ashing for 4-6 h at 550°C. Caps were cleaned by soaking for 1 h in dilute HCl followed by nanopure rinses. Water samples for DOC, CDOM, and absorbance were filtered through pre-ashed glass microfiber filters (Whatman GF/F) in the field and stored

in the dark at 4°C or frozen (Fe) until analysis. Samples for chlorophyll *a* were filtered in the field (Whatman GF/F) and stored frozen in foil until analysis by fluorometry following acetone extraction.

Laboratory procedures. UV/Vis absorbance scans from 250 to 700 nm were obtained in 1- and/or 5-cm quartz cells on filtered samples using a UV-1601PC UV-visible spectrophotometer (Shimadzu Sci. Instr., Inc.). Results were used to compute: a_{440}, $SUVA_{254}$, and values of the spectral slope, *S*, over various wavelength ranges. Filtered water samples were analyzed for DOC using a Shimadzu TOC Vcpn analyzer (Shimadzu Sci. Instr., Inc.), calibrated with dilutions of a potassium hydrogen phthalate solution (Sigma Aldrich, Inc.). Blanks were prepared by mimicking the procedure with ultrahigh purity water and analyzing DOC to confirm that contamination did not occur in sample handling.

Secchi depth data. To increase the number and range of SD data for our analysis we obtained results from Minnesota's well-established Citizen Lake Monitoring Program (CLMP), administered by the Minnesota Pollution Control Agency (MPCA), which collects SD data on lakes throughout the state. We selected imagery (described below) that included a large number of well monitored lakes with SD data collected within 3 days of image acquisition.

3.2 Satellite imagery acquisition and processing

Nearly cloud-free imagery was downloaded from the EROS Center, Sioux Falls, South Dakota. For SD comparisons, we used a Landsat 7 image of path 27 rows 27 through 30 from September 1, 2008, for which 309 SD measurements were available for model calibration, and a Landsat 8 image of path 27 rows 27 through 30 for August 22, 2013, for which 311 SD measurements were available. For CDOM model development and comparison, we used Landsat 8 image of path 27 row 27 for September 16, 2013 and a Landsat 7 image of path 27 row 27 for

September 24, 2013. Image processing was based on methods we developed previously (Olmanson et al., 2001; Kloiber et al., 2002ab; Olmanson et al., 2008 & 2011; Chipman et al., 2009; Brezonik et al., 2015). We used Leica Geosystems ERDAS Imagine 2015 and ESRI ArcGIS 10.2 for image processing. Image preprocessing included layer stacking and removing areas with missing pixel values for some bands and areas obscured by clouds and haze. Because each image was calibrated individually with field data, we did not perform atmospheric correction or normalization of the image brightness data.

Once image preprocessing was complete, a "water-only" image was produced by performing an unsupervised classification based on ISODATA clustering. Because water features have spectral characteristics distinct from terrestrial features, water pixels were grouped into one or a few distinct classes that could be easily identified. We then masked out terrestrial features to create a water-only image, performed an unsupervised classification on this image, and generated spectral signatures of each class. We used these signatures, along with the location where the pixels occurred, to differentiate open water from shallow water where sediment and/or macrophytes affected spectral response. Shallow water pixels tend to have high spatial variability compared to open water pixels and are easily identified. Based on this analysis, we removed the affected shallow water pixels to create an "open water" image.

Spectral-radiometric data from the "open water" images were used to develop relationships with measured water quality data. For Landsat images used to retrieve SD information, we used a lake polygon layer with polygons delineating lakes or lake basins (Olmanson et al., 2001) to expedite the process. The signature editor in ERDAS Imagine was used to extract spectral data for all the lakes on the image. Using a histogram analysis procedure (Chipman et al., 2004; Olmanson et al., 2001), we calculated the mean band values from the middle 50% of the pixels

from each lake and imported them into Microsoft Excel. To avoid reliance on samples with only a few pixels, lakes with fewer than six pixels were removed. For Landsat images used to model CDOM levels, we delineated relatively large (8 to 319 pixels) sample locations in spectrally uniform areas from the imagery manually and used the signature editor in ERDAS Imagine to extract the spectral data. The larger sample size (versus relying on one or a few pixels) has been shown to significantly increase correlation strength, as measured by r^2 and the standard error of the estimate (Kloiber et al. 2002a, Lillisand et al. 1983) in legacy Landsat imagery. Ratios for all band combinations were calculated, and field data were linked to the appropriate lake.

3.3 Model development

To develop models to estimate SD from the imagery products, we performed forward step-wise regressions of the band data sets using the JMP Pro 11 statistical software package (SAS Institute, Inc.). The log-transformed value of SD was the dependent variable, and single bands and band ratios were the independent variables. From these results, we used the two independent variables that contributed most to the regression fit and applied them in a second multiple regression using the general form:

$$ln(SD) = b_1(band\ or\ combination) + b_2(band\ or\ combination) + b_3 \quad [3]$$

where b_1-b_3 are coefficients fit to the calibration data by the regression analysis, ln(SD) is the natural logarithm (ln) of SD for a given lake, and "band or combination" is the image radiance value for the selected lake pixels in the best fit band or band ratios.

CDOM retrieval equations were also developed by regression analysis using the calibration data we gathered in 2013 and 2014; no other sources of CDOM data were available for Minnesota. Regressions were performed in Systat and JMP Pro 11. We explored a wide variety

of model forms involving ETM+ and OLI bands and band ratios using both a_{440} and ln(a_{440}) as the dependent variables.

4. Results

4.1 Water quality calibration data sets

SD data from the MPCA data base for the September 1, 2008 Landsat 7 image had a range of 0.15 to 8.84 m (n = 309) with mean and median values of 2.75 and 2.54 m, respectively. SD data for the August 22, 2013 Landsat 8 image had a range of 0.02 to 8.53 m (n = 311) and mean and median values of 3.04 and 3.00 m, respectively. The ranges are close to the observed ranges for SD in lakes across the state of Minnesota (Olmanson et al., 2013).

A statistical summary of water quality characteristics for the 28 CDOM calibration sites shows a wide range of CDOM values (a_{440} of 0.5-25.1 m^{-1}). Mean (± standard deviation) and median values for a_{440} in the data set are 8.9 ±7.3 and 7.0 m^{-1}, respectively. Selected sites are thought to be broadly representative of the approximate range of a_{440} in northern and central Minnesota. They were not selected on a random basis, however, and extrapolation of the mean, standard deviation and range to the entire population of lakes and rivers in the region would not be appropriate. The wide range of CDOM in the database is useful in determining the best models for each sensor.

As noted above, we sampled sites that included a broad range of chlorophyll concentrations and suspended sediments so that the calibration database would include systems where light absorption and scattering by algae and mineral suspended sediment (MSS) was important, as well as lakes where CDOM was the only important optical property. The ranges of chlorophyll *a* (1.5-25.5 μg/L), TSS (0.7-1012.2 mg/L), MSS (0.0-

873.9 mg/L) and SD (0.5-5.0 m) in the site data set indicate that this was achieved. The data set thus includes moderately eutrophic lakes that are optically complex systems. The ranges for SD and chlorophyll are typical for lakes in the Minnesota ecoregions where the data were collected (Olmanson et al., 2008) and optically complex riverine systems with high MSS. Corresponding mean (± standard deviation) and median values for chlorophyll *a*, TSS, MSS and SD in the data set are 7.2 ± 6.2 and 5.2 μg/L, 75.7 ± 234.2, 3.6 mg/L, and 72.7 ± 213.7, 2.3 mg/L, 1.71 ± 1.27 and 1.25 m, respectively.

4.2 Model Development for SD

The September 1, 2008 Landsat 7 ETM+ image was used previously as part of a Minnesota statewide water clarity assessment for 2008, which can be accessed at water.umn.edu. For this image we used the legacy model involving the ETM+ blue and red bands (bands 1 and 3, hereafter denoted E1 and E3): $\ln(SD) = b_1(E1/E3) + b_2E1$, which has been used for routine monitoring of water clarity (SD) in Minnesota (Olmanson et al. 2008), Wisconsin (Greb et al., 2009; Chipman et al., 2004), and Michigan (Fuller et al., 2004 & 2011). A strong relationship was found between ln(SD) and the spectral radiometric responses in the image ($R^2 = 0.82$; RMSE = 0.35).

Stepwise regression was used to identify the best SD model for the August 22, 2013 Landsat 8 image, with all the bands and band ratios, including the new ultra-blue and narrower NIR bands, as potential independent variables. The best SD model for Landsat 8 used the OLI blue, red and ultra-blue bands (bands 2, 4, and 1, respectively, hereafter denoted O2, O4, and O1): $\ln(SD) = b_0 + b_1(O2/O4) + b_2O1$ ($R^2 = 0.82$; RMSE = 0.334). This model was nearly identical

with $\ln(SD) = b_0 + b_1(O2/O4) + b_2O2$ ($R^2 = 0.817$; RMSE = 0.337), which is similar to the legacy model used for the Landsat 7 image.

4.3 Model Development for CDOM

Landsat 7. Overall, Landsat 7 did not perform as well as Landsat 8 (see discussion below), but when the entire dataset was used, a few models did work as well as previous studies (e.g., Kutser et al., 2005a; Brezonik et al., 2005). The best fit for Landsat 7 was obtained with a two-variable model involving two band ratios: $\ln(a_{440}) = b_0 + b_1(E2/E3) + b_2(E3/E4)$ ($R^2 = 0.74$), where E2, E3 and E4 are the radiance in ETM+ bands 2, 3 and 4). Four additional models had reasonable fits ($R^2 > 0.6$), including a model involving the band ratio E2/E4 and band E3 with $R^2 = 0.67$ (Table 1). The model coefficients in Table 1 are specific to this data set and incorporate atmospheric effects for the images used. A comparable set of calibration data would be needed to determine the coefficients in future studies.

A regression of $\ln(a_{440})$ versus ln(E2/E3) yielded a poor fit for Landsat 7 ($R^2 = 0.25$) when all 25 data points were included. This model is essentially a natural logarithm transform of the widely used model of Kutser et al. (2005ab). Inspection of the plot of $\ln(a_{440})$ versus ln(E2/E3) (green/red bands) (Figure 1) showed that all five sites on the St. Louis River estuary (SLRE), which flows into western Lake Superior near Duluth, Minnesota, were large outliers. These sites had high levels of mineral suspended solids that likely contribute to their status as outliers. Excluding these sites from the analysis yielded a data set containing 20 sites (average $a_{440} = 8.7$ m^{-1}; range = 0.5-22.6 m^{-1}) of less optically complex waters which may be typical for inland lakes in many areas. We examined a wide variety of potential band and band ratio models for retrieval of $\ln(a_{440})$ and a_{440} using this subset (Table 2) and found 8 model forms that yielded $R^2 > 0.7$ An

additional 11 model forms had R^2 in the range 0.6-0.7. The best fit was obtained with a two-variable model: $\ln(a_{440}) = b_0 + b_1(E2/E3) + b_2(E2)$ ($R^2 = 0.83$), which is similar to the best model reported by Brezonik et al. (2005). A model involving the two band ratios E1/E3 and E2/E3 was almost as good ($R^2 = 0.83$), and a model involving only the E2/E3 band ratio yielded $R^2 = 0.80$. The Kutser-like model, $\ln(a_{440})$ vs. ln(E2/E3), had only a slightly poorer fit ($R^2 = 0.79$). In contrast, analogous models using band ratios with E4 in the denominator gave R^2 of ~0.6. Overall, it appears that Landsat 7 can provide reasonable predictive relationships for a_{440} using a variety of model forms, some of which include the NIR band for data sets involving a rather wide range of CDOM levels and turbidity. Relationships break down, however, for some models, including the "Kutser" model, in waters with high mineral suspended solids and in some high CDOM waters.

Landsat 8. Better relationships were obtained for CDOM retrieval with the OLI sensor than with ETM+. For example, a two-variable model form, $\ln(a_{440}) = b_0 + b_1(O3/O5) + b_2(O4)$, yielded $R^2 = 0.82$ when all 28 data points were included. Models with $\ln(a_{440})$ as dependent variables and ln(O2/O5) plus O1 as independent variables yielded $R^2 = 0.79$. When O2 was substituted for the second term, the R^2 was reduced to 0.73, but this form allowed closer comparison with a corresponding "legacy" Landsat 7 model: $\ln(a_{440}) = b_0 + b_1(E1/E4) + b_2(E1)$, which for the Landsat 7 image had an R^2 of only 0.62. In contrast, the ln-transformed model of Kutser et al. (2005ab), $\ln(a_{440})$ vs. ln(O3/O4), had an R^2 of only 0.24, and the best one-variable ln-ln model using all the data was $\ln(a_{440})$ vs. ln(O2/O5), $R^2 = 0.48$. A plot of $\ln(a_{440})$ versus ln(O3/O4), which is comparable to the Landsat 7 model $\ln(a_{440})$ versus ln(E2/E3) for the same sites available in the Landsat 7 image (Figure 2), showed that the five SLRE sites also were large outliers for the Landsat 8 data.

The SLRE sites plus SW Bay of Sturgeon Lake and two high CDOM lakes (Johnson & Section 11) that were not in the Landsat 7 data set were removed to yield a data set with 20 sites (average a_{440} = 9.7 m^{-1}; range 0.5-25.1 m^{-1}) coincident to the subset used for Landsat 7. For this less optically complex subset a wide variety of potential band and band ratio models were examined for retrieval of ln(a_{440}) and a_{440} using this data set (Table 3). The additional ultra-blue band (O1) in the OLI sensor resulted in a larger number of potential band combinations than was the case with the 4 bands (3 visible and 1 NIR) of the ETM+ sensor. A total of eight model forms had $R^2 > 0.8$, an additional 5 had R^2 between 0.7 and 0.8, and 10 had R^2 between 0.6 and 0.7. The best fit models (R^2 of 0.82-0.83) involved two band ratios, all with band O4 (red) as denominator terms, but models involving just the O3/O4 ratio (green/red) were nearly as good (R^2 of 0.818-0.820). Inclusion of O1, O2, or O3 as independent terms did not improve the O3/O4 relationship; in each case the second term was not statistically significant. In addition, the ln-linear model (ln(a_{440}) vs. O3/O4) had the same R^2 as the ln-ln model (ln(a_{440}) vs. ln(O3/O4)).

We also examined additional models with the full data sets that include the high suspended sediment and high CDOM waters and found a two-variable model: $\ln(a_{440}) = b_0 + b_1(O3/O4) + b_2(O4/O5)$ ($R^2 = 0.76$) for Landsat 8 and comparable model, $\ln(a_{440}) = b_0 + b_1(E2/E3) + b_2(E3/E4)$ ($R^2 = 0.74$), for Landsat 7 worked reasonably well for both sensors. Having models that work with optically complex waters will be important for regional measurements when optical properties are unknown.

The generally strong performance of the ETM+ sensor in this study in spite of its lower radiometric sensitivity and signal to noise ratio probably can be explained by the approach we used to retrieve water quality information from the imagery. In particular, use of a large number of pixels essentially provides more precise estimates of spectral radiometric data than individual

pixels provide. To illustrate this statistically we compared the USGS Surface Reflectance Landsat products for the OLI and ETM+ sensors using a sample of 196 pixels from a spectrally similar area in Lake Vermillion. The improved signal to noise ratio of the OLI sensor is evident with significantly lower ± standard deviations and coefficients of variation (CV) than the ETM+ sensor (Table 4). This is further illustrated in the CDOM maps where the Landsat 7 map shows more noise, (Figures 5 and 6) than the Landsat 8 map (Figure 7 and 8).

5. Discussion and Conclusions

For SD we found strong relationships with both sensors, and the OLI sensor did not appear to be better than ETM+ even for the higher clarity lakes in our datasets (Figures 3 and 4). Although the higher radiometric sensitivity of OLI should allow for more accurate measurements on lakes with high clarity (> ~6-8 m) this may have been mitigated by our approach of using many pixels as discussed above. The range of SD values in our calibration dataset (0.15-8.8 m) is suitable for most Minnesota lakes, but with only 9 and 18 measurements > 6 m for Landsat 7 and 8, respectively, more measurements of water clarity in the most oligotrophic waters are needed to determine whether OLI is more accurate than ETM+ in measuring water clarity in lakes with SD > ~ 6-8 m.

Overall, it appears that both Landsat 7 and Landsat 8 can provide reasonable predictive relationships for a_{440} using a variety of model forms for data sets involving low to moderate CDOM levels, but relationships broke down in waters with high inorganic suspended sediment and some high CDOM waters when some models, including the Kutser nonlinear ratio model, were used. Therefore, it may be necessary to either limit their use to more optically simple waters with low to moderate CDOM levels or select models that work equally well in simple and optically complex waters. How best to determine when simpler models are no longer adequate is

an issue that needs further analysis. In this study models using the new Landsat 8 ultra-blue and narrower NIR band worked best for the full dataset, which included optically complex waters; however, the comparable model did not work as well for Landsat 7 indicating that the new bands improve CDOM measurements. Two-variable models using the green/red and red/NIR bands worked reasonably well for both Landsat 7 and Landsat 8 and represented the high CDOM and the SLRE waters with high mineral suspended solids well. Use of the model that worked best for each sensor produced maps with comparable levels of CDOM. The Landsat 7 map (Figure 5 and 6) shows more noise, however, than the Landsat 8 map (Figure 7 and 8) and has missing data because of the malfunction of the scan line corrector.

Although further research with a larger dataset is needed to determine the overall best model for each sensor and dominant water quality characteristics, this study indicates that Landsat 7 can be used for historic measurements of CDOM, which is important to determine whether long term changes in CDOM levels have been occurring. The OLI sensor's ultra-blue and narrower NIR bands, along with improved radiometric and signal to noise ratios, seem to provide substantial improvements that will open up opportunities for accurately measuring and mapping CDOM and understanding the controls over water clarity and carbon cycles at regional to global scales.

Acknowledgments

We thank Sandra Brovold, Michelle Rorer, Nolan Kleijan, and Adam Worm, Dept. of Ecology, Evolution, and Behavior, Univ. of Minnesota, Luke Loken, Univ. of Wisconsin-Madison, and Chip Small, Univ. of St. Thomas, and others who assisted with sample collection and lab assistance with the 2013 and 2014 field data, and the Lake Superior National Estuarine Research Reserve and research coordinator Shon Schooler for sampling assistance on the St.

Louis River Estuary. We also thank Pamela Anderson Supervisor of the Water Quality Monitoring Unit, MPCA and the CLMP volunteers for the SD data. PLB thanks the Univ. of Minnesota Office of the Vice President for Research (UMOVPR) and UM Retirees Association for an award from the Professional Development Grants Program for Retirees that provided financial support. JCF acknowledges support from the Minnesota Sea Grant College Program supported by the NOAA office of Sea Grant, United States Department of Commerce, under grant No. R/RegHCE-09-12. LGO and MEB acknowledge support from the UMOVPR for funding under the U-Spatial: Spatial Science and Systems Infrastructure grant and the Univ. of Minnesota Agricultural Experiment Station.

References

Brezonik, P. L., Olmanson, L. G., Finlay, J. C. & Bauer, M. E. (2015). Factors affecting the measurement of CDOM by remote sensing of optically complex inland waters. *Remote Sensing of Environment, 157*, 199-215. DOI 10.1016/j.rse.2014.04.033.

Brezonik, P. L., Menken, K., & Bauer, M. E. (2005). Landsat-based remote sensing of lake water quality characteristics, including chlorophyll and colored dissolved organic matter (CDOM). *Lake & Reservoir Management, 2*, 373-382.

Carlson, R. E. (1977). A trophic state index for lakes. *Limnology & Oceanography, 22*, 361-369

Chipman, J. W., Olmanson, L. G., & Gitelson, A. A. (2009). Remote sensing methods for lake management: a guide for resource managers and decision-makers. Developed by North American Lake Management Society in collaboration with Dartmouth College, University of Minnesota, University of Nebraska and University of Wisconsin for the United States Environmental Protection Agency.

Chipman, J. W., Lillesand, T. M., Schmaltz, J. E., Leale, J. E., & Nordheim, M. J. (2004). Mapping lake water clarity with Landsat images in Wisconsin, USA. *Canadian Journal of Remote Sensing, 30*, 1−7.

Davies-Colley,R. J., & Vant, W. N. (1987). Absorption of light by yellow substance in freshwater lakes. *Limnol. Oceanogr., 32*, 416-425.

Ficek, D., Zapadka, T., & Dera, J. (2011). Remote sensing reflectance of Pomeranian lakes and the Baltic. *Oceanologia, 53*, 959-970.

Fuller, L. M., Aichele, S. S., & Minnerick, R. J. (2004). Predicting water quality by relating Secchi-disk transparency and chlorophyll *a* measurements to satellite imagery for Michigan inland lakes, August 2002: U.S. Geological Survey, Scientific Investigations Report 2004–5086.

Fuller, L. M., Jodoin, R. S., & Minnerick, R. J. (2011). Predicting lake trophic state by relating Secchi-disk transparency measurements to Landsat-satellite imagery for Michigan inland lakes, 2003–05 and 2007–08: U.S. Geological Survey Scientific Investigations Report 2011–5007, 36 p.

Greb, S. R., Martin A. A., & Chipman, J. W. (2009). Water clarity monitoring of lakes in Wisconsin, USA using Landsat. Proceedings of 33rd International Symposium of Remote Sensing of the Environment. Stresa, Italy.

Houser, N. J. (2006). Water color affects the stratification, surface temperature, heat content, and mean epilimnetic irradiance of small lakes. *Can. J. Fish. Aquat. Sci*. **63**: 2447-2455.

Kloiber, S. M., P. L. Brezonik, L. G. Olmanson, & M. E. Bauer. (2002a). A procedure for regional lake water clarity assessment using Landsat multispectral data. *Remote Sensing of Environment, 82*, 38-47.

Kloiber, S. M., P. L. Brezonik, & M. E. Bauer. (2002b). Application of Landsat imagery to regional-scale assessments of lake clarity. *Water Research, 36*, 4330-40.

Kutser, T. (2012). The possibility of using the Landsat image archive for monitoring long time trends in coloured dissolved organic matter concentration in lake waters. *Remote Sensing of Environment, 123*, 334-338.

Kutser, T., Pierson, D. C., Kallio, K. Y., Reinart, A., & Sobek, S. (2005a). Mapping lake CDOM by satellite remote sensing. *Remote Sensing of Environment*, *94*, 535-540.

Kutser, T., Pierson, D. C., Tranvik, L., Reinart, A., Sobek S., & Kallio, K. (2005b). Using satellite remote sensing to estimate the colored dissolved organic matter absorption coefficient in lakes. *Ecosystems, 8*, 709-720. DOI 10.1007/s10021-003-0148-6.

Lillesand, T. M., Johnson, W. L., Deuell, R. L., Lindstrom, O. M., & Meisner, D. E. (1983). Use of Landsat data to predict the trophic state of Minnesota lakes. *Photogrammetric Engineering and Remote Sensing,* 49, 219– 229.

Menken, K., Brezonik, P. L., & Bauer, M. E. (2006). Influence of chlorophyll and humic color on reflectance spectra of lakes: implications for measurement of lake-water properties by remote sensing. *Lake & Reservoir Management*, *22*(3), 179-190.

Olmanson, L. G., Brezonik, P. L. & Bauer, M. E. (2015). Remote sensing for regional lake water quality assessment: capabilities and limitations of current and upcoming satellite systems, chapter 5, *Advances in watershed science and assessment*. Springer. The Handbook of Environmental Chemistry Volume 33, DOI 10.1007/978-3-319-14212-8_5.

Olmanson, L. G., Brezonik, P. L. & Bauer, M. E. (2013). Geospatial and temporal analysis of a 20-year record of Landsat-based water clarity in Minnesota's 10,000 lakes. *Journal American Water Resources Association, 50,* 1-14. DOI 10.1111/jawr.12138.

Olmanson, L. G., Brezonik, P. L. & Bauer, M. E. (2011). Evaluation of medium to low resolution satellite imagery for regional lake water quality assessments, *Water Resources Research, 47*, W09515, DOI 10.1029/2011WR011005.

Olmanson, L. G., Bauer, M. E., & Brezonik, P. L. (2008). A 20-year Landsat water clarity census of Minnesota's 10,000 lakes, *Remote Sensing of Environment*, *112*(11), 4086–4097,

Olmanson, L. G., Kloiber, S. M., Bauer, M. E. & Brezonik, P. L. (2001). Image processing protocol for regional assessments of lake water quality. Public Report Series #14. Water Resources Center and Remote Sensing Laboratory, University of Minnesota, St. Paul, MN, 55108, 15 p.

Thurman, E. M. (1983). Determination of aquatic humic substances in natural waters. U.S. Geol. Surv. Paper Hydrol. Sci. W2262, p. 47-52.

University of Minnesota, Remote Sensing and Geospatial Analysis Laboratory. Remote Sensing of Water, Lake Browser http://water.umn.edu/. Last accessed April 15, 2015.

Wilkinson, G. M., Pace, M. L., & Cole, J. J. 2013. Terrestrial dominance of organic matter in north temperate lakes. *Global Biogeochem. Cycles* **27**. doi: 10.1029/2012GB004453.

Table 1. Summary of regression results for various band and band ratios models to predict ln(a_{440}) using the September 16, 2013 Landsat 8 and September 24, 2013 Landsat 7 image using all available ground data (28 and 25 respectively) from surface water locations.

		Equation coefficients $y = b_0 + b_1(x_1) + b_2(x_2)$				
Independent Variables[a]	**R^2**	**b_0**	**b_1**	**b_2**	**Large Leverage**[b, d]	**SEE**[c]
Landsat 7 ln(a_{440}) models						
lnE2/E3, lnE3/E4	0.74	11.1	-13.2	-7.2	1	0.49
E2/E3, E3/E4	0.74	20.3	-10	-2.4	1,2	0.49
E2/E4, E3	0.67	8.8	-3.3	0.11	1,2	0.49
ln(E1/E4), E1	0.62	23.5	-12	-0.07	1,2	0.60
E1/E4, E1	0.61	16.1	-2.4	-0.06	1,2	0.60
ln(E1/E4)	0.60	21.9	-13		1,2	0.60
Landsat 8 ln(a_{440}) models						
O3/O5, O4	0.82	23.5	-36	0.004	2	0.43
ln(O2/O5), O1	0.79	-21.9	-75.8	0.005	1,2	0.46
O3/O5, O3	0.78	23.7	-70.3	0.010	2	0.47
lnO3/O4, lnO4/O5	0.76	8.3	-50	-19.0	2	0.50
O3/O4, O4/O5	0.74	67.4	-44.8	-15.0	2	0.51
ln(O2/O5), O2	0.73	-9.4	-73.3	0.005	1,2	0.53
O2/O5, O2	0.73	38	-51.4	0.005	1,2	0.52
O3/O4, O3	0.66	52.6	-33	-0.002	2	0.58
O1/O4, O2/O4	0.64	20.3	121.1	-149.5	1,2	0.60
O1/O4, O3/O4	0.61	35.6	16.4	-52.0	2	0.63
O3/O4, O2	0.61	58.4	-27.9	-0.003	1,2	0.63

[a] Numbers refer to Landsat 7 ETM+ bands and Landsat 8 OLI bands. Commas separate terms in a given model.

[b] Case 1 (Lake Superior, near Duluth) had large leverage in models where noted; case 2 (SLRE 10 Allouez Bay) had large leverage in models where noted (see Brezonik et al. 2015 for site map).

[c] Standard error of estimate.

[d] Similar regression equations and fits were obtained when the high-leverage data points were removed.

Table 2. Summary of regression results for various band and band ratios models to predict a_{440} or ln(a_{440}) using the September 24, 2013 Landsat 7 image and ground data from 20 surface water locations.

Independent Variables[b]	R^2	Equation coefficients[a] $y = b_0 + b_1(x_1) + b_2(x_2) + b_3(x_3)$ b_0	b_1	b_2	b_3	Large Leverage[c, d]	Outlier[c]	RMSE
ln(a_{440})								
E1/E3, E2/E3	0.827	14.62	2.77	-14.21				0.43
E1/E4, E2/E4, E3/E4	0.817	2.21	1.01[ns]	-5.84	5.36	18		0.46
E2/E4, E3/E4	0.807	4.03	-4.52	4.932		18		0.46
E2/E3, E2	0.832	17.54	-8.53	-0.142		18		0.43
E2/E3, E1	0.808	19.1	-9.09	-0.104[ns]		18	15	0.46
E1/E3, E2	0.801	21.02	-4.05	-0.333		18		0.46
E1/E3, E1	0.637	23.56	-2.69	-0.313		18		0.63
E2/E4, E1	0.653	17.57	-1.57	-0.219		18		0.62
E2/E4, E2	0.608	12.08	-1.47[ns]	-0.189[ns]		18		0.65
E1/E4, E2	0.641	14.37	-1.19[ns]	-0.220		18		0.63
E1/E4, E1	0.637	19.07	-1.24	-0.224[ns]		18		0.63
E2/E3	0.791	16.04	-10.8			18	15	0.46
ln(E2/E3)	0.784	5.75	-14.5				15	0.47
a_{440}								
E1/E3, E2/E3	0.676	64.88	19.2[ns]	-74.1				3.1
E1/E4, E2/E4, E3/E4	0.668	-9.62	13.9[ns]	-39.2	30.08	18		3.3
E2/E4, E3/E4	0.601	15.49	-21.0	24.2		18		3.5
E2/E3, E1	0.616	71.08	-52.77	0.124[ns]		18	15	3.4
E2/E3, E2	0.641	81.01	-41.0	-0.595[ns]		18		3.3
E2/E3	0.615	74.72	-50.69			18	15	3.3

[a] Superscript [ns] after a coefficient means it was not statistically significant.

[b] Numbers for independent variables refer to Landsat 7 ETM+ bands. Commas separate terms in a given model.

[c] Case 18 (Lake Superior, near Duluth) had large leverage in models where noted; case 15 (South Sturgeon L.) was an outlier, where noted.

[d] Similar regression equations and fits were obtained when the high-leverage data points were removed.

[e] The following ln(a_{440}) model forms had R^2 values < 0.6: E1/E4, E2/E4; E2; E1/E4; ln(E2/E4); and ln(E1/E4).

[f] The following a_{440} model forms had R^2 values < 0.6: E1/E4, E2/E4; E2/E4, E2; E2/E4, E1; E1/E3, E1; E1/E4, E1; E2/E4.

Table 3. Summary of regression results for various band and band ratios models to predict ln(a_{440}) or a_{440} using the September 16, 2013 Landsat 8 image and ground data from 20 surface water locations.

Independent Variables[b]	R^2	Equation coefficient[sa] $y = b_0 + b_1(x_1) + b_2(x_2)$ b_0	b_1	b_2	Large Leverage[c, d]	Outlier[c]	RMSE
ln(a_{440}) models[d]							
O1/O4, O2/O4	0.830	29.2	109.3	-143.2	16,18		0.44
O1/O4, O3/O4	0.821	48.4	2.6[ns]	-45.7	18		0.46
O2/O4, O3/O4	0.820	48.8	2.6[ns]	-45.8	18		0.46
O3/O4, O1	0.820	46.6	-43.7	0.000[ns]	16		0.46
O3/O4, O3	0.819	49.6	-42.5	0.000[ns]			0.46
O3/O4, O2	0.818	48.3	-43.3	0.000[ns]	16		0.46
O3/O4	0.818	49.0	-42.9				0.45
ln(O3/O4)	0.818	6.3	-47.5				0.45
O3/O5, O3	0.796	28.4	-72.7	0.009			0.49
O2/O5, O2	0.729	32.4	-56	0.006	11,16		0.56
O1/O5, O2/O5	0.667	34.4	59.5	-89.5	16,18		0.62
O1/O5, O1	0.665	30.1	-52.4	0.006	11,16		0.62
O2/O5, O3/O5	0.621	47.0	-22.1	-11.7[ns]	16,18		0.66
O1/O5, O3/O5	0.600	49.7	-16.8	-17.9	16,18		0.68
a_{440} models[e]							
O3/O4, O1	0.753	162	-294	0.02	16		3.5
O3/O4, O2	0.738	193	-308	0.02	16	14	3.6
O3/O5, O3	0.730	127	-496	0.074			3.7
O3/O4, O3	0.666	259	-271	-0.007[ns]			4.1
O2/O4, O3/O4	0.660	284.3	42.5[ns]	-300	18		4.1
O1/O4, O3/O4	0.659	279.2	30.8[ns]	-286	18		4.2
O3/O4	0.648	286	-252				4.1
O2/O5, O2	0.630	80.3[ns]	-397	0.064	11,16		4.3
O1/O5, O1	0.611	50.8[ns]	-359	0.061	11,16		4.4

[a] Superscript [ns] means coefficient was not statistically significant.

[b] Numbers for independent variables refer to Landsat 8 OLI bands. Commas separate terms in a given model.

[c] Cases 11 (Sandy River L.), 16 (L. Superior), 18 (L. Vermilion, Big Bay), had large leverage and case 14 (South Sturgeon L.) was an outlier in models where noted.

[d] Similar regression equations and fits were obtained when the high-leverage data points were removed.

[e] The following ln(a_{440}) model forms had $R^2 < 0.6$ (in order of decreasing R^2): O3/O5, O1; O3/O5, O2; ln(O2/O5); O2/O5; ln(O3/O5); O3/O5; ln(O2/O4); ln(O1/O5); O1/O5; O1/O4; ln(O1/O4); and O3.

[f] The following a_{440} model forms had $R^2 < 0.6$ (in order of decreasing R^2): O1/O4, O2/O4; O3/O5, O2; O3/O5, O1; O1/O5, O2/O5; O2/O4, O2; O2/O5, O3/O5; O1/O5, O3/O5; O3/O5; O2/O5; O1/O4, O1; O1/O5; and O3.

Table 4. Lake Vermillion summary statistics for a 196 pixel sample from the Landsat OLI and ETM+ sensors to illustrate the improved signal to noise ratio of the OLI sensor. Units are in surface reflectance with a 0.0001 scale factor.

September 16, 2013 OLI					
OLI	Min	Max	Mean	SDV	CV %
1	72	96	83.61	4.69	5.60
2	99	113	106.28	2.63	2.48
3	158	175	167.02	2.97	1.78
4	108	120	113.88	2.73	2.39
5	32	43	37.03	1.98	5.34
6	1	8	4.40	1.35	30.67
7	-2	5	1.85	1.38	74.24

September 24, 2013 ETM+					
ETM+	Min	Max	Mean	SDV	CV %
1	118	268	202.63	26.02	12.84
2	182	290	233.65	23.40	10.01
3	66	183	131.56	24.50	18.63
4	37	142	95.58	25.83	27.03
5	-68	80	19.22	22.51	117.08
7	-65	89	17.74	28.03	158.05

Standard deviation (SDV)

Coefficient of variation (CV)

List of Figure Captions

Figure 1. Plot of in situ ln(a_{440}) vs. ln(B2/B3) Landsat 7 ETM+. The SLRE outliers are shown in blue.

Figure 2. Plot of in situ ln(a_{440}) vs. ln(B3/B4) Landsat 8 OLI. The SLRE outliers are shown in blue.

Figure 3. Plot of in situ ln(SD) vs. Landsat 7 ETM+ derived ln(SD).

Figure 4. Plot of in situ ln(SD) vs. Landsat 8 OLI derived ln(SD).

Figure 5. Distribution of lake CDOM levels in northern MN near Ely based on part of the September 9, 2013 Landsat 7 image.

Figure 6. Distribution of lake CDOM levels in Pike and Big Bay of Lake Vermillion using the September 24, 2013 Landsat 7 image.

Figure 7. Distribution of lake CDOM levels in northern MN near Ely based on part of the September 16, 2013 Landsat 8 image.

Figure 8. Distribution of lake CDOM levels in Pike and Big Bay of Lake Vermillion using the September 16, 2013 Landsat 8 image.

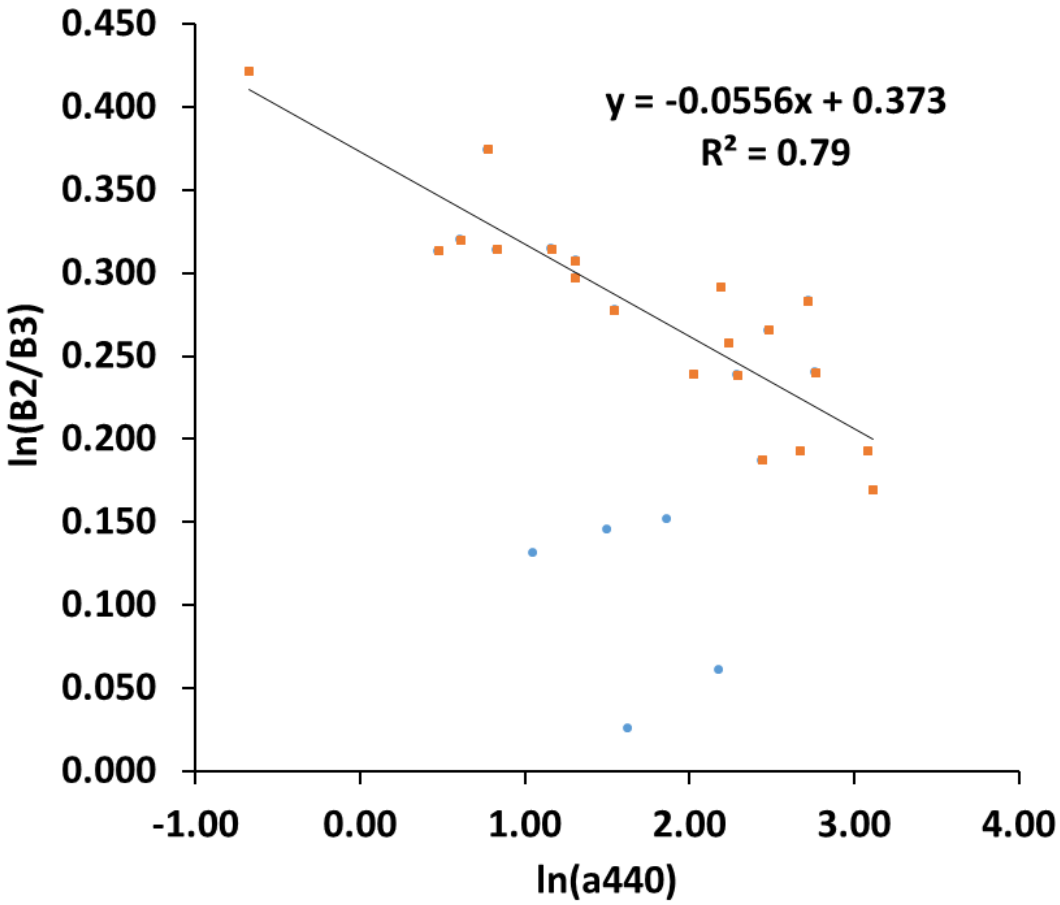
y = -0.0556x + 0.373
R² = 0.79
ln(B2/B3)
ln(a440)
0.450
0.400
0.350
0.300
0.250
0.200
0.150
0.100
0.050
0.000
-1.00
0.00
1.00
2.00
3.00
4.00

Fig. 1

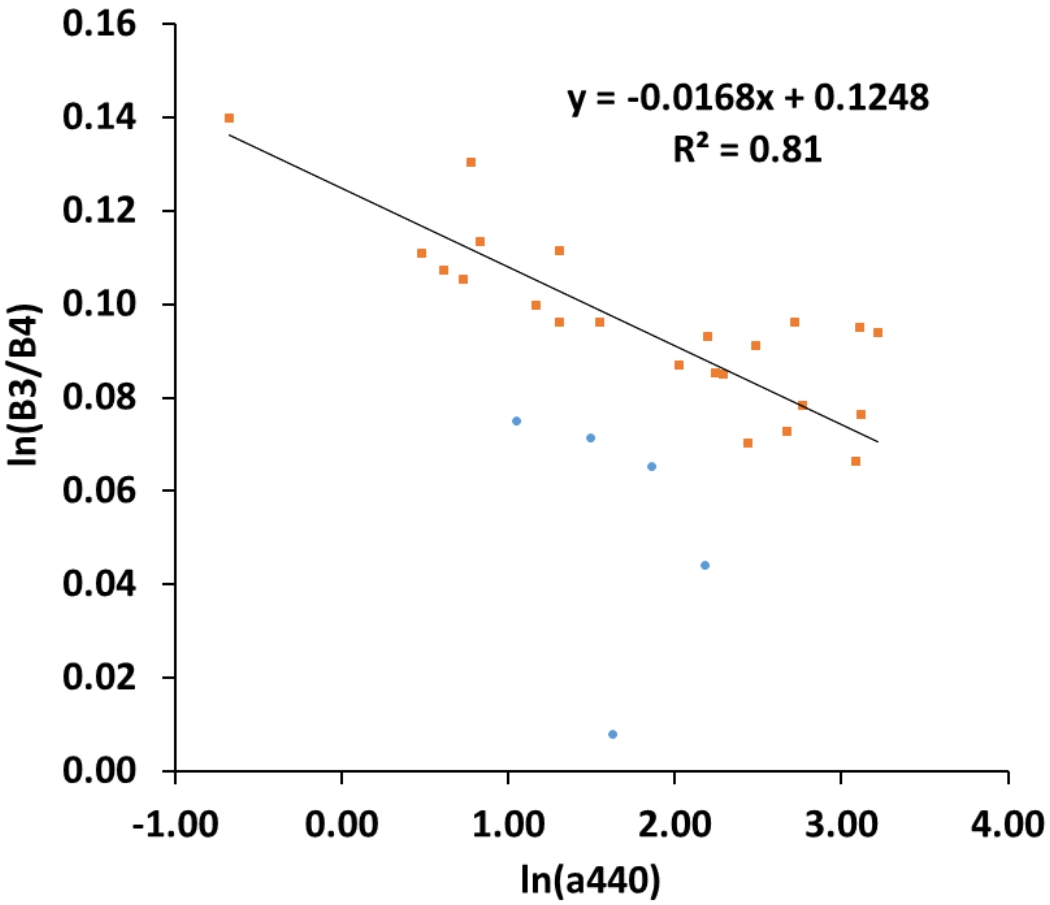
y = -0.0168x + 0.1248
R² = 0.81
ln(B3/B4)
ln(a440)
0.16
0.14
0.12
0.10
0.08
0.06
0.04
0.02
0.00
-1.00
0.00
1.00
2.00
3.00
4.00

Fig. 2

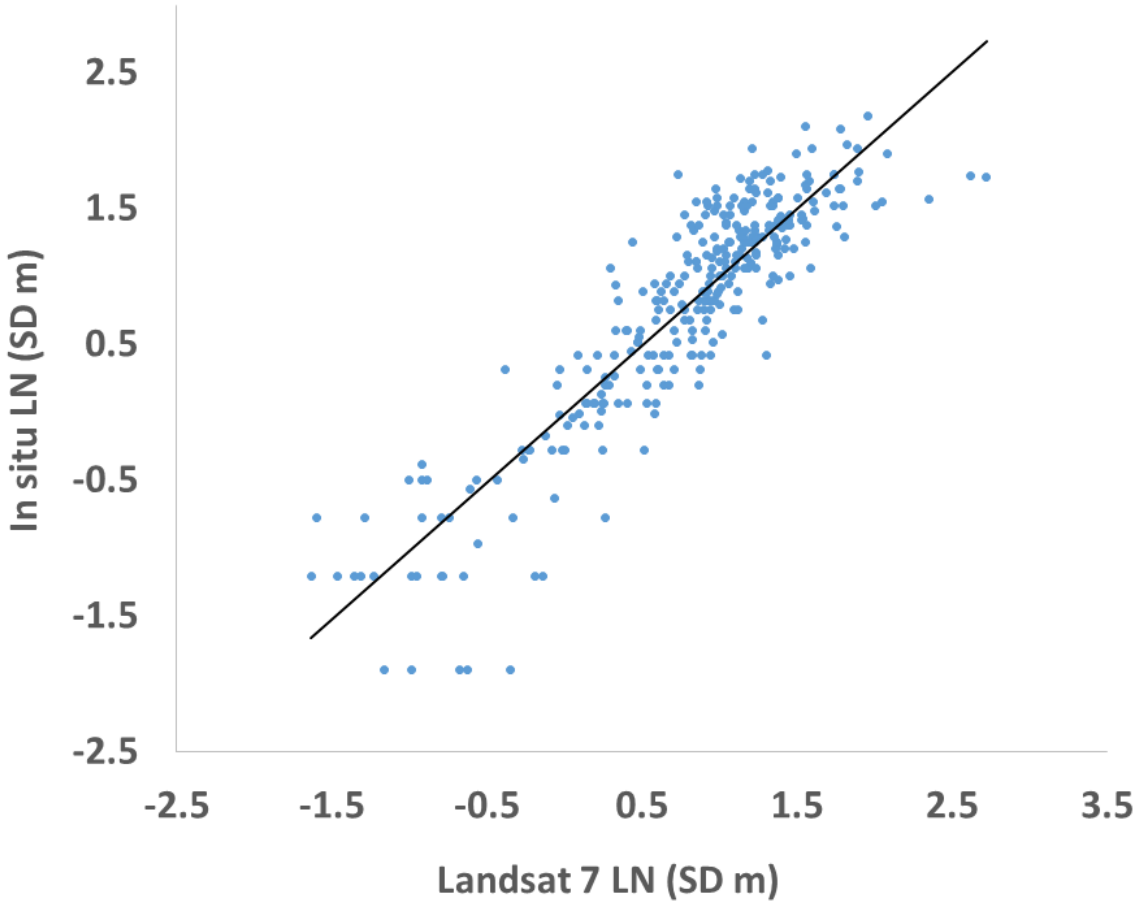
2.5
1.5
0.5
-0.5
-1.5
-2.5
In situ LN (SD m)
-2.5
-1.5
-0.5
0.5
1.5
2.5
3.5
Landsat 7 LN (SD m)

Fig. 3

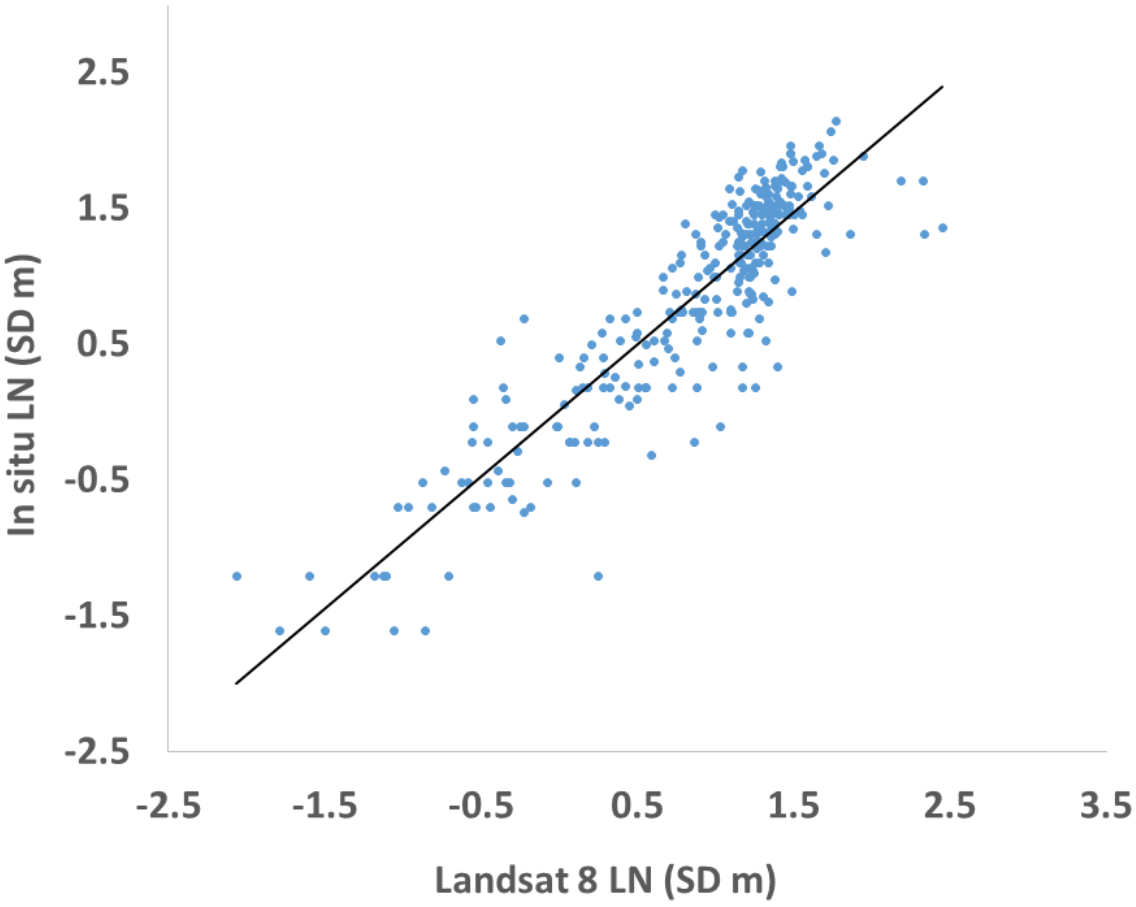
2.5
1.5
0.5
-0.5
-1.5
-2.5
In situ LN (SD m)
-2.5
-1.5
-0.5
0.5
1.5
2.5
3.5
Landsat 8 LN (SD m)

Fig. 4

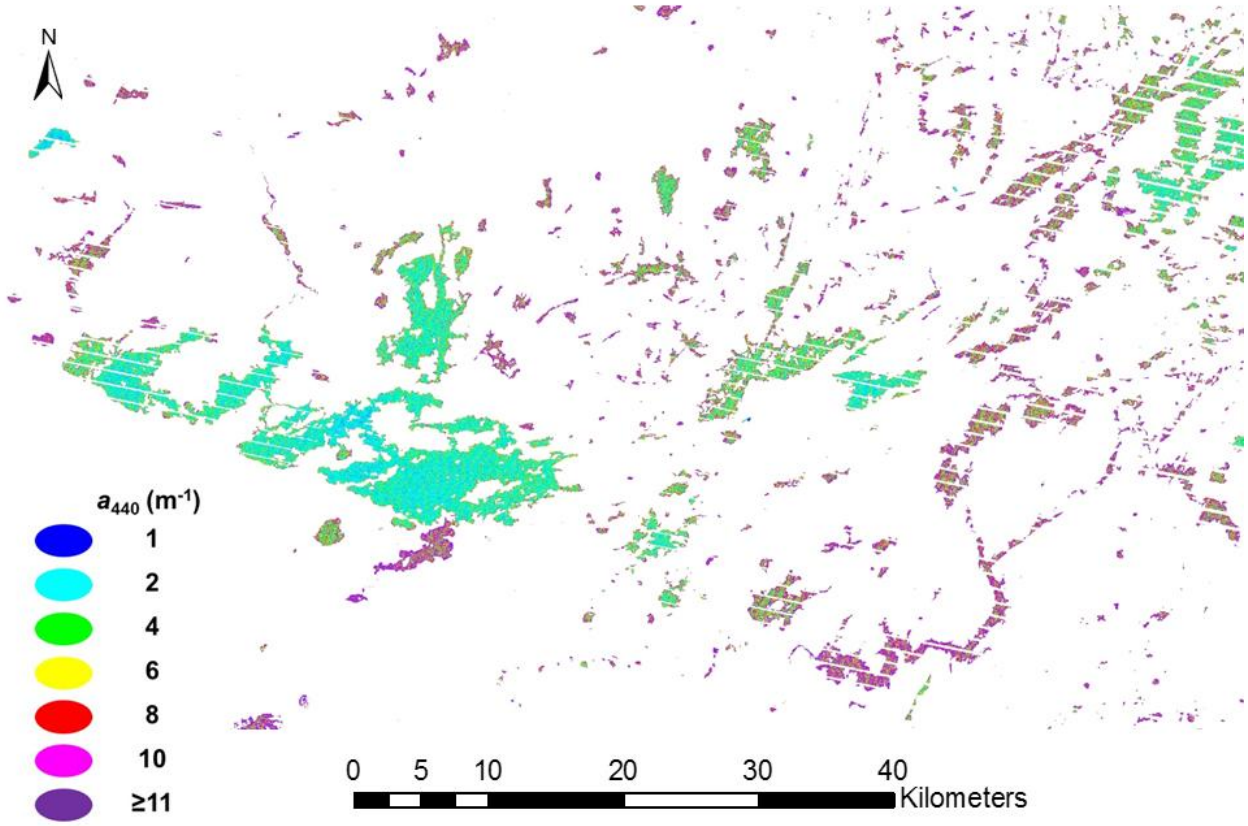

Fig. 5

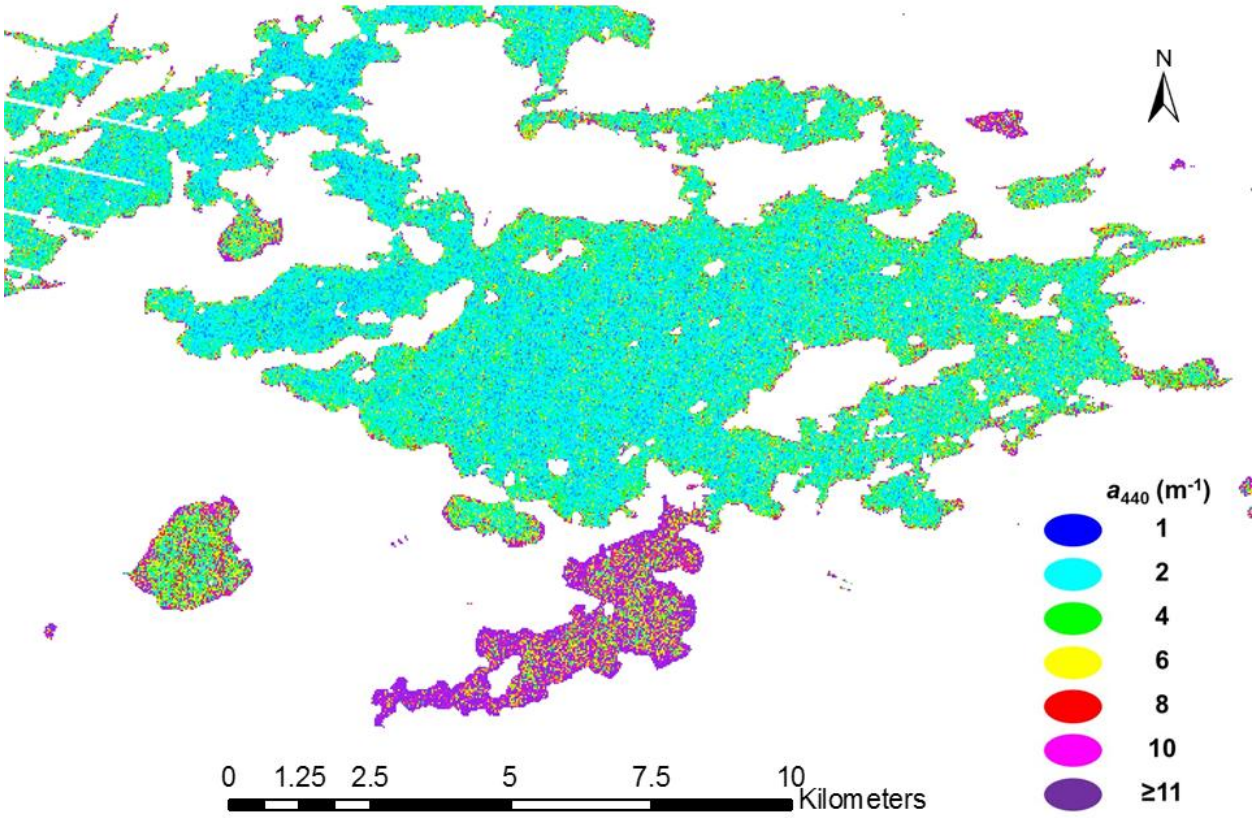

Fig. 6

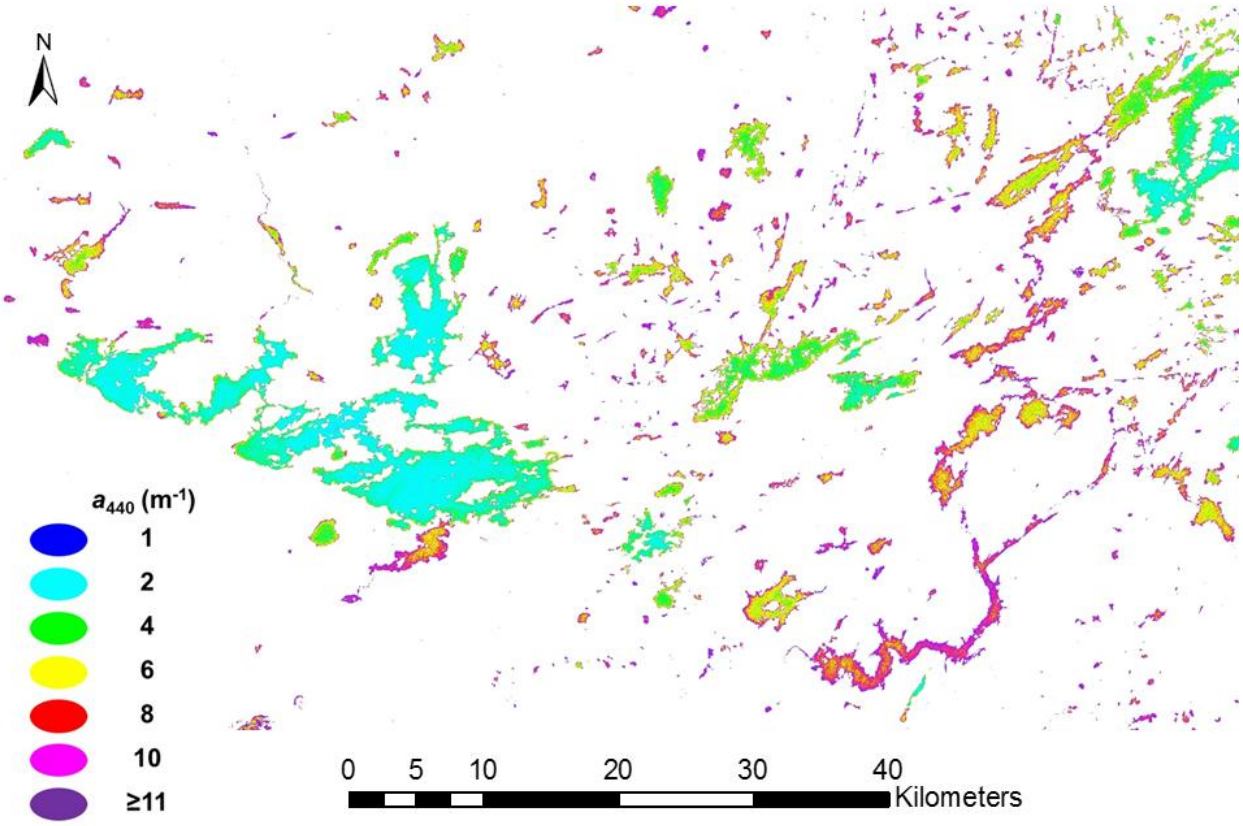

Fig. 7

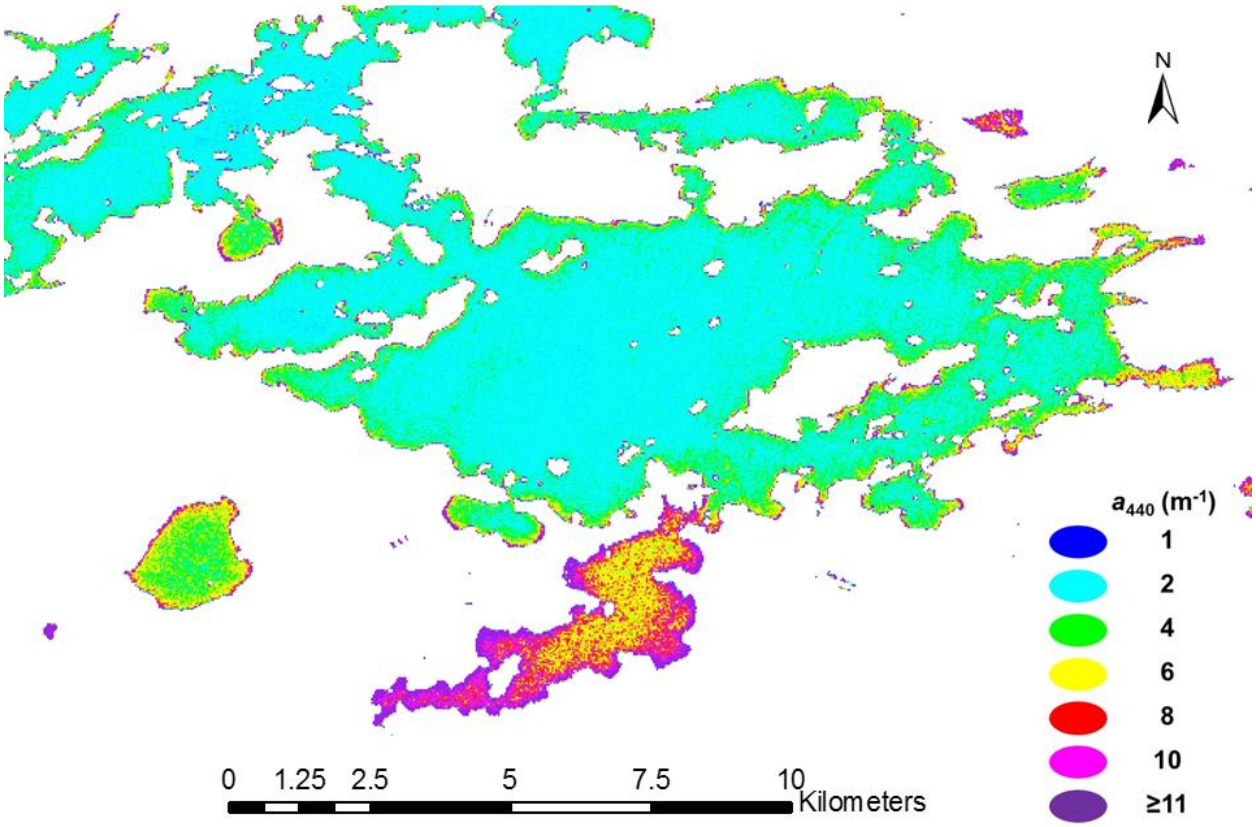

Fig. 8

Research Highlights

Landsat 7 and 8 data were compared for mapping CDOM and clarity of inland lakes

Landsat 8 was better for estimating CDOM than Landsat 7 in optically complex waters

Landsat 8 was only a slight improvement over Landsat 7 for measuring water clarity

Landsat 7 and 8 will continue and enhance remote sensing of regional water quality